AIR-WATER TWO-PHASE FLOW EXPERIMENTAL AND NUMERICAL ANALYSIS IN A CENTRIFUGAL PUMP

Q. Si[1], G.Bois[2], K. Zhang[1], J. Yuan[1]

(1. National Research Center of Pumps, Jiangsu University, Zhenjiang, China, 212013;
2. LML, UMR CNRS 8107, ENSAM-Lille Campus, France -ATTAG Chairman

ABSTRACT

The paper presents experimental and numerical investigations performed on a single stage, single-suction, horizontal-orientated centrifugal pump in air-water two-phase non condensable flow conditions. Experimental test loop allows performing controlled values of air void fraction for different water flow rates for a several rotational speeds. Global pump heads and efficiencies are obtained for several inlet air void fraction values at different rotating speeds up to pump performance breakdown. Similarity laws under two-phase flow condition are investigated at three selected rotating speeds. Numerical calculations are also performed using URANS approach including *k-e* turbulence and inhomogeneous two-phase models for nominal rotational speed, the results of which are used to understand some specific experimental results.

KEYWORDS: Two-Phase flow, Centrifugal pump, Performance

NOMENCLATURE

b: impeller blade width
D: Diameter
H: Pump head;
n: rotational speed
P: Shaft power
Q: Water flow rate
R: Radius
Re: Reynolds number $R_e = u_2 \cdot \frac{R_2}{\nu}$
Z: impeller blade number
u: Circular velocity
α: local air void fraction
φ: Flow coefficient $\varphi = Q/(2\pi \cdot R_2 \cdot b_2 \cdot u_2)$
ρ: Density of mixed fluid
$\rho = \rho_{water} \times (1-\alpha) + \rho_{air} \times \alpha$
ν: water cinematic viscosity
ω : angular velocity
η: Global efficiency of the pump $\eta = \frac{\rho g Q_{water} H}{P}$
ψ: Head coefficient $\psi = gH/(u_2)^2$
ψ_t: Theoretical head coefficient $\psi_t = \psi / \eta$
Ωs*:* Specific speed
$\Omega s = \omega \cdot \frac{Q^{0.5}}{(gH)^{0.75}}$
IAVF: Inlet air void fraction $IAVF = \frac{Q_{air}}{Q_{air} + Q_{water}} inlet$
d: design condition
o: outlet
s: suction
rpm: revolution per minute
1: Impeller pump inlet
2: Impeller pump outlet

INTRODUCTION

Centrifugal pumps are widely used in industrial applications, such as in waste water treatment, oil industry, food production, nuclear power, heating installations, shipbuilding industry or chemical industry. In some case, air will enter into the liquid conveying pump. Centrifugal pumps are commonly designed for single phase flow only. It is already well known that pump both head and efficiency will decrease under two-phase mixture condition compared to single-phase one. The degree of the degradation depends on geometrical, physical and thermal conditions. Moreover, air-water flow may even cause damage to the pump. Thus, it is of great interest for engineers to understand and disclose the air-water flow in centrifugal pumps.

There is a continuing engineering and scientific request for advanced studies on pumps in two-phase operation. Experimental testing included measuring pressure heads, power consumption, flow rates, flow visualization, bubble size measurement in two phase flows, and void fraction distribution have been done by Murakami and Minemura (1974a, 1974b), Kim et al. (1985), Sato et al. (1996), Suryawijaya (2001), Thum et al. (2006), Thomas et al. (2015). However, most of centrifugal pump impeller geometries that have been studied for two-phase regimes are designed with two dimensional blade sections. Modern computational fluid dynamics meanwhile offers some capacity to simulate the flow characteristic. However, reliable two-phase flow simulations are still quite difficult due to the complexity of the flow and again the lack of suitable validation data and benchmark experiments. A two-phase semi-empirical approach was first developed by Mikielewicz et al. (1978) for a given specific speed type of centrifugal pumps. Several one dimensional models based on homogenous gas-liquid mixture have also been proposed by Minemura et al. (1985, 1995), Furuya et al. (1985), Clarke and Noghrehkar (1995). These models can be considered to be valid for low values of void fraction (max. 6%) and so, far from surge operating conditions. Numerical simulations using URANS approach have been also performed in order to determine local phenomena more precisely in such flow pattern. Caridad and Kenyery (2004) simulated two phase flow in an electrical submersible pump (ESP) using a 3D CFD model. Barrios and Prado (2009) studied the dynamic behavior of the multiphase flow inside an ESP by setting the bubble size through high speed camera measurement results. This numerical method get better fit to experiment results in ESP research field, which will help us apply it to centrifugal pumps investigation.

In the present paper, experimental and numerical comparisons results are presented on two-phase flow performance in a centrifugal pump designed with 3D impeller shape. Two different experimental procedures are presented which aim is to prevent too much result scattering due to flow instabilities that usually occur with two phase flow pump behavior. Numerical results have been performed using inhomogeneous model (instead of usually homogeneous model), for which each fluid possesses its own flow field and the fluids interact via interphase transfer terms and compared with overall experimental ones.

PUMP GEOMETRY AND TEST RIG ARRANGEMENT

A commercial single stage, single-suction, horizontal-orientated low specific speed ($\Omega s = 0.68$) centrifugal pump from manufacturer Grundfos was used to process the measurement, whose casing is typically combined with a spiral-volute vaneless annulus. We suppose the best efficiency operating point as the design one. The design parameters of the pump are shown in Table 1.

Table 1 Pump Parameters

Parameters	Value	Parameters	Value
Design flow rate Q_d/m^3 h^{-}	50.6	Suction pipe diameter D_s/mm	65
Design Head H_d/m	20.2	Outlet pipe diameter D_o/mm	50
Rotation speed n_d/ r min^{-1}	2910	Impeller inlet diameter D_1/mm	79
Blade number Z	6	Impeller outlet diameter D_2/mm	140
Outlet Blade width b_2/mm	15.5	Base diameter of volute D_3/mm	150

Test rig is shown on Figure 1. As shown in this open loop (upstream and downstream tanks are open to atmosphere), a compressor allows air injection into the mixer by means of rake tubing with calibrated small diameter holes . Air flowrates are measured by micro-electro mechanical systems flow sensors, which supplies volume air flowrate values under standard conditions (25 ℃elcius, 101325 Pascals). Air bubbles can exhaust to atmosphere and the left pure water runs to the upstream flow meter. Water flowrate is measured by an electromagnetic flow meter set between upstream tank and the mixer. Pump head and global efficiency are also obtained following ISO 9906-2012

rules. The inlet pipe loop is horizontal and part of it is transparent. This allows a global rough view of bubbles size. At this step, only air volume flow rate is measured. Bubble diameter distribution including bubble number per volume at pump inlet is not available. Measurements are performed using the followed procedures: a constant void fraction is set by changing the throttle vane position and consequently obtained the corresponding water flow rate. Measurement biggest uncertainties calculated by instrument precision are+- 1,6 % relative error for pump head and +- 0.5% of air void fraction evaluation due to the effects of pump flow oscillations.

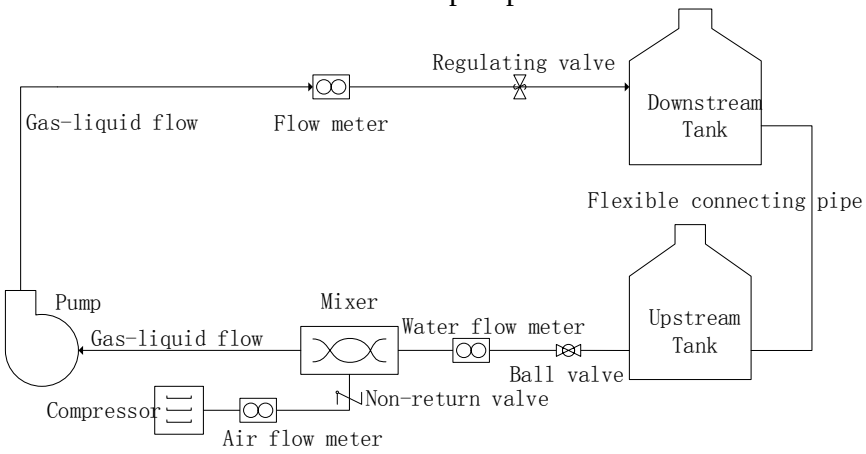

Figure.1 Test rig

Pump performance measurements are performed for several impeller rotating speeds in order to plot all results using usual dimensionless coefficients for similarity laws investigation. For air-water two phase flow measurements, the test loop inlet condition is set with 2m water head inside the upstream tank. Four air injection tubes are oriented with the same direction as the water flow, using 0.5mm diameter holes around the mixer pipe. The water flow rate is kept constant, and the air injecting flow rate is adapted to keep the air void fraction at constant values up to 10% and even more. Such pump performance measurements under two phase flow are performed for three selected rotating speed.

NUMERICAL SIMULATION MODLING

Calculation domain and meshes

The pump domain is divided into component parts such as the suction inlet, ring, pump impeller, volute and chamber to build a numerical model for a complete pump, as shown in Figure 2. This process would allow each mesh to be individually generated and tailored to the flow requirements in that particular component. The influence of boundary conditions was investigated to discard any effect on the numerical results, particularly on the inlet and outlet part. We extend these two parts to assume that the flow closed to inlet and outlet parts were in a fully developed condition.

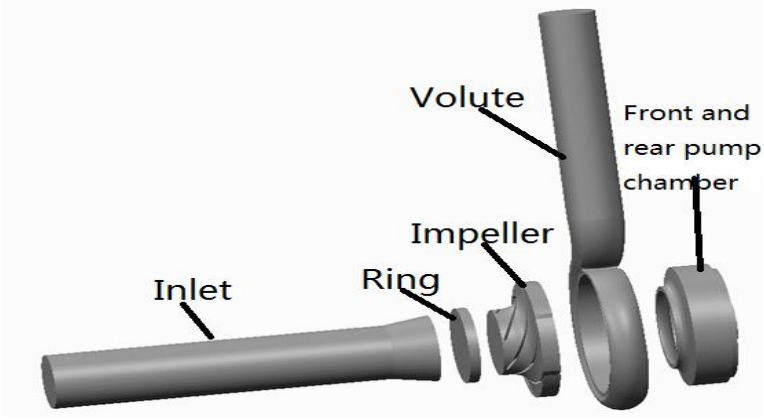

Figure.2 3D view of pump model of numerical domain

The grids for the computational domains were generated using the grid generation tool ICEM-CFD 14.5 with blocking method. The independence of the solutions from the number of grid elements is proven by simulating the flow field with different numbers of grid elements. Finally, the resulting pump model consists of 2775915 according to the results given in table 2a. Structured hexahedral cells were used to define the inlet, impeller ring, impeller, chamber and volute domains (see Table 2b).

The grid details in the rotating domain and the volute wall are partially shown in Figure 5.

Tab.1a. Grid number dependence on overall performances

Grid Number N	Head H/m	Efficiency η/%
1467332	21.518	76.321
1998779	20.806	73.776
2218839	20.595	73.421
2548031	20.603	73.529
2775915	20.655	73.823
2894787	20.654	73.801
3172155	20.657	73.775

Tab.1b. Mesh distribution inside the numerical domain

Domain	Grid number
inlet	422 604
Impeller ring	42 240
Impeller	950 976
Chamber	433 656
Volute	926 439
TOTAL	2 775 915

The grid details inside the impeller and in the volute wall are partially shown in Figure 3.

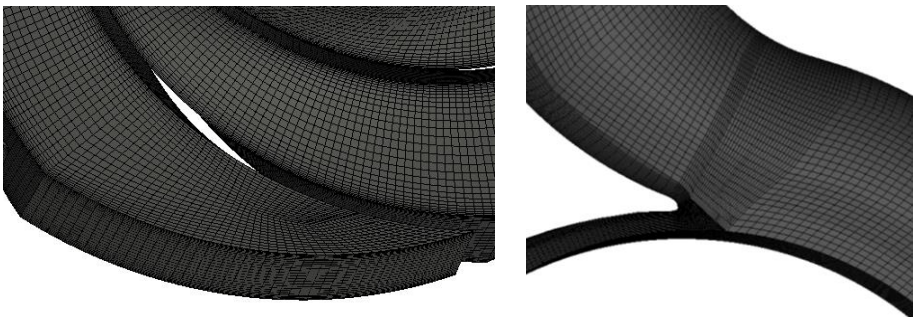

Figure.3 Details of grid view. (Left side: impeller detail- Right side: volute tongue detail)

Boundary condition and numerical models

Three-dimensional URANS equations are solved using the *k-e* turbulence model, with boundary conditions of total pressure at the inlet and mixture mass flow at the outlet. Smooth wall conditions are used for the near-wall function. Inhomogeneous model also named the inter-fluid transfer model is chosen to adapt the Eulerian-Eulerian multiphase flow. In this model each fluid possesses its own flow field and the fluids interact via interphase transfer terms. Thus, this model provides one solution field for each of the separate phases. Transported quantities interact via interphase transfer terms. Furthermore, particle model is applied for the interphase transfer terms,

which is suitable for modeling dispersed multiphase flow problems such as the dispersion of gas bubbles in a liquid. Bubble diameters can be set as 0.1mm or 0.2mm.

The interface between the impeller and the casing is set to "transient rotor-stator" to capture the transient rotor-stator interaction in the flow, because the relative position between the impeller and the casing was changed for each time step with this kind of interface. The chosen time step (Δt) for the transient simulation is 1.718×10^{-4}s for nominal rotating speed, which corresponds to a changed angle of 3 °. Within each time step, 20 iterations were chosen and the iteration stops when the maximum residual is less than 10^{-4}. The convergence criterion for the transient problem is when the result reaches its stable periodicity. Ten impeller revolutions are needed for each operational condition, and the last four revolutions results are kept for analysis.

EXPERIMENTAL AND NUMERICAL OVERALL PUMP PERFORMANCE RESULTS

Inlet and outlet total head is deduced from wall static pressure measurement and a one dimensional evaluation of kinetic pressure obtained from the volume flow rate measurements. Theoretical total head coefficient can be also obtained through global pump efficiencies, assuming no initial swirling flow at impeller inlet section. Pump performance results from numerical simulation is calculated by the average of one impeller revolution.

Single phase pump characteristics

Using head and flow coefficient from similarity laws, the following results on overall pump performances are shown in Figures 4, respectively for total head coefficient and theoretical total head. The following theoretical total head curves are built using classical head coefficient ψ_{th}. Five different rotational speeds have been chosen from nominal one (2910 rpm) to the lowest one (1300 rpm).

The Reynolds number value, based on the impeller outlet radius, is relatively small for the last three values of the pump rotational speed of 1800, 1500 and 1300 rpm. If the relative outlet velocity should have been chosen, these values will be below 1×10^{6}. This is probably the reason why the results on Figures 4 (a) do not follow what expected according to similarity laws for these rotational speeds. However, the theoretical total head coefficients curve, Figure 4 (b), exhibits a single curve for all rotational speeds. As a consequence, two phase flow measurements were carried out with three rotational speeds: 2910 rpm (nominal rotational speed), 2300 and 1800 rpm (assumed to be the critical rotating speed according to Reynolds number value).

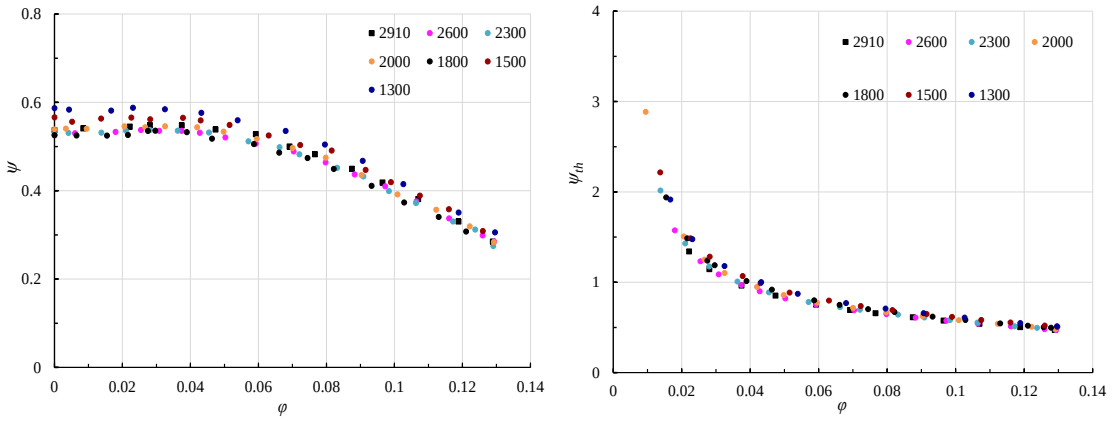

(a) Head (b) Theoretical head

Figure.4 Pump head curve at different rotating speed under single phase condition

Two phase (air-water) pump characteristics

In the following, all results are presented for constant inlet air void fraction (IAVF) and water flow rate values, for three different rotational speeds excluding the two smaller ones for which Reynolds number values are below the critical one.

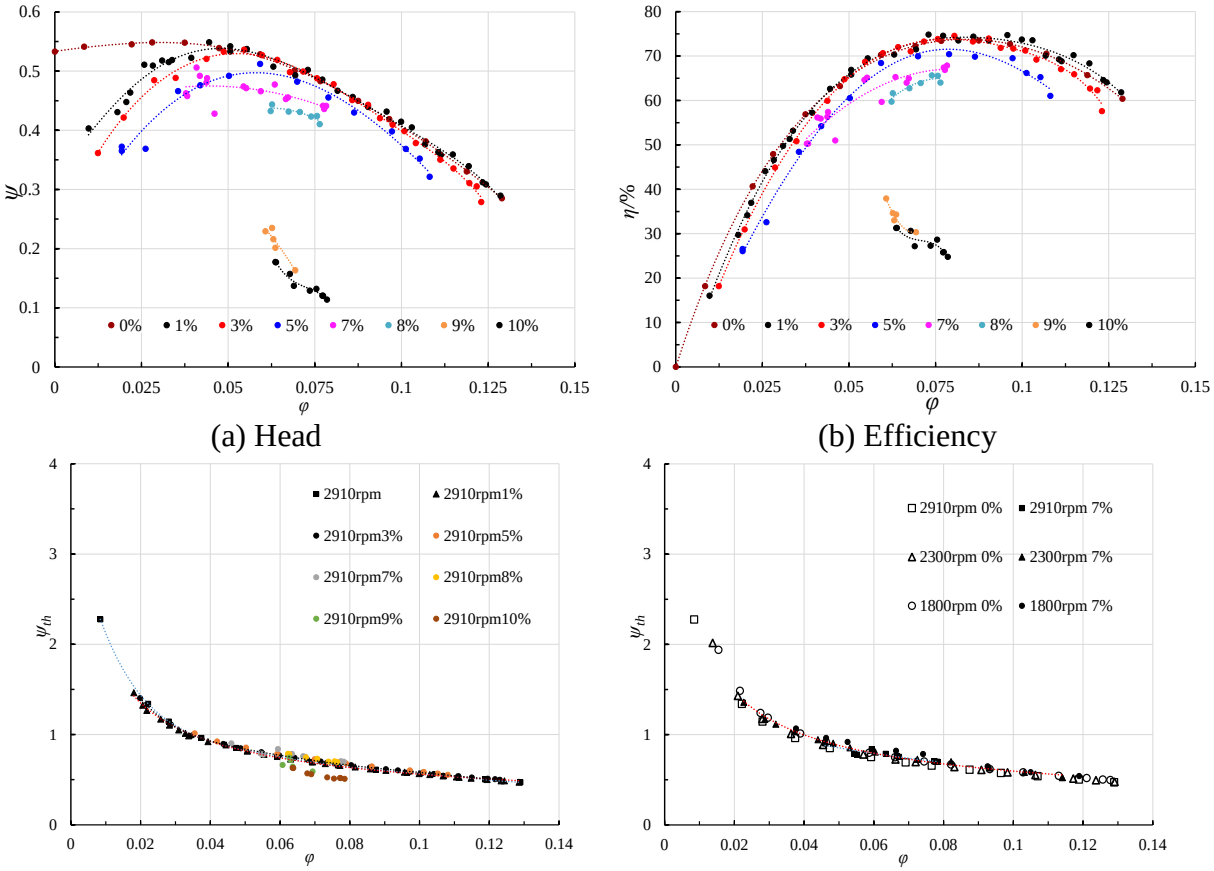

(a) Head (b) Efficiency

(c) Theoretical head at 2910rpm (d) Theoretical head under IAVF=0 and 7%

Figure 5. Pump performance curves under two phase flow conditions

Figure 5a and b show the pump performances under different IAVF for the nominal rotational speed of 2910 rpm. The maximum relative errors in the head and efficiency calculations were 3.8% and 1.3%, respectively. Void fraction value is estimated within 0.4% error.

It can be seen, as already pointed out by several previous researchers, that pump performances start to be significantly lower when void fraction is above 3% or 5%, depending on the water flow rate. A decrease of 20% of head compared with single phase shut-off conditions is achieved for all water flow rates below optimum conditions for void fraction going up to 7%. Lowest void fraction up to 10% can be achieved without important pump surging for water flow rates coefficient around 0.06~0.077 (32~40 m^3/h). This value does not correspond to optimum pump efficiency point 0.087, which is reached for 45m^3/h. On the efficiency curves, one can observed that maximum efficiency locations are displaced towards lower water flow rates when void fraction is increasing. This can be attributed to blockage effects at impeller inlet section which may affect the incidence angle values. Pump head and efficiency curves at the other two rotating speed give the same trend, but present the different values, which will discuss next.

Figure 5 (c) show a remarkable result, for which a unique curve is found using corrected two phase head and flow coefficients up to void fraction value of 8%. For the last two air void fraction, values of theoretical results are smaller than the IAVF below 8%. This may result from a change on the two phase relative flow angle at impeller outlet section, slip factors, or a bigger uncertainty on head measurement due to flow instabilities that start to be quite important for such void fraction values. Figure 5 (d) shows theoretical dimensionless head curves under IAVF=0 and 7% at rotating speed of 2910rpm, 2300rpm, 1800rpm. It exhibits a single curve for all rotational speeds. Moreover,

curves at other IAVF that don't appear at this manuscript limited by the space also present the same law, which means that theoretical head is independent of fluid density duo to the two-phase flow. This result is an important one, since it validates all semi-empirical and one dimensional model assumptions that have been used for most of existing approaches that can be seen in the literature for such pump geometry with bubbly flow regime.

A second experimental set concerns the real head evolutions, obtained respectively for 0, 1, 3, 5 and 7% of air void fraction for three different rotational speeds. Total head coefficients versus flow coefficients are presented in Figure 6. Seen from the results, the similarity laws can also be applied for air-water two phase flow conditions corresponding to the bubbly flow regime when IAVF are quite small (less than 3%). Pump heads exhibit increased difference when the IAVF increase. Moreover, results at 2300rpm and 1800rpm always show lower values than that at 2910rpm.

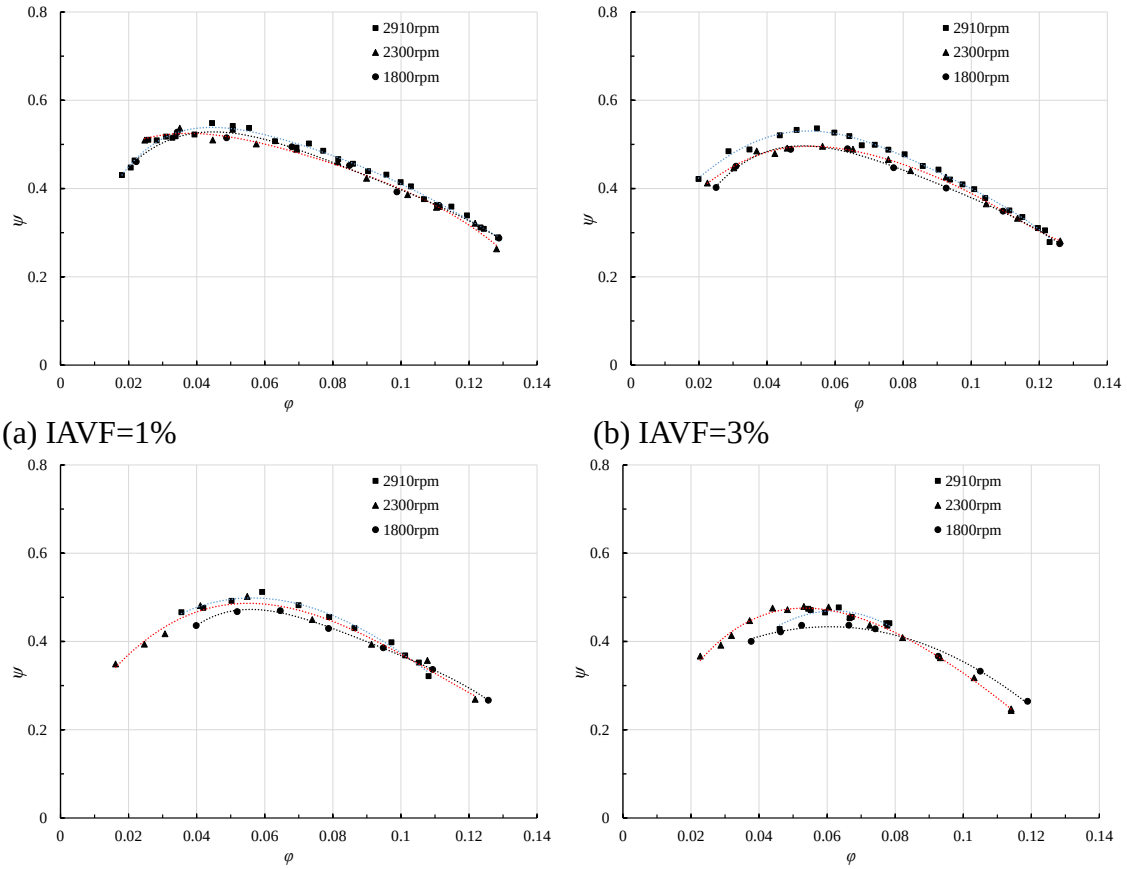

(a) IAVF=1% (b) IAVF=3%

(c) IAVF=5% (d) IAVF=7%

Figure 6. Pump head coefficients comparison at different IAVF.

Pump performance degradation ratio ψ/ψ_0 has been obtained from previous results and plotted versus IAVF for three different flow coefficients, as shown in Figure 7. In each figure, the rotational speed is set as a parameter. It seems that rotational speed influences the head drop rate of the pump. The degradation ratio is biggest at 1800rpm under all three flowrate and become small when increase the rotating speed. The curves keep quite stable and close to 1 up to IGVF=5% at two bigger rotating speed under flow coefficients φ=0.077 and 0.058. When flow coefficient is decreasing, the head drop is more pronounced for decreasing rotational speeds.

Compared to existing experiments such as presented in Minemura et al.,(1985) paper, it can be pointed out that the head coefficient ratio remains at a quite high level for the present pump (even for IAVF=10%, with a small decrease of 5~6%) taking into account measurement accuracy. For higher values of IAVF (between 8 and 10%), the present experimental results do not follow the model proposed by Minemura et al(1985) and are close to the initial Furuya (1985)'s model. In fact, the flow coefficient is an important parameter to deal with. So, it is believed that the flow incidence

at impeller inlet must appear when building a model, because this may change the local void fraction which is an important parameter in order to predict the usual sudden head pump drop.

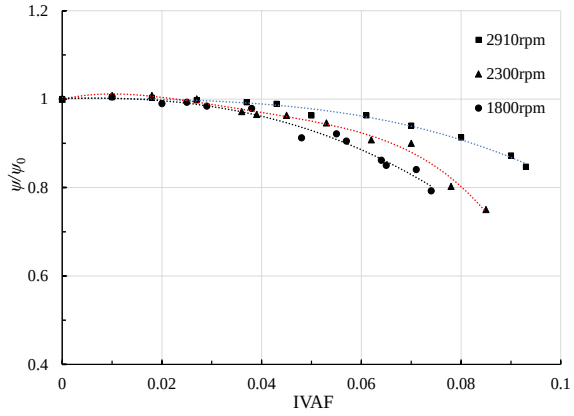

(a) Flow coefficient φ=0.077

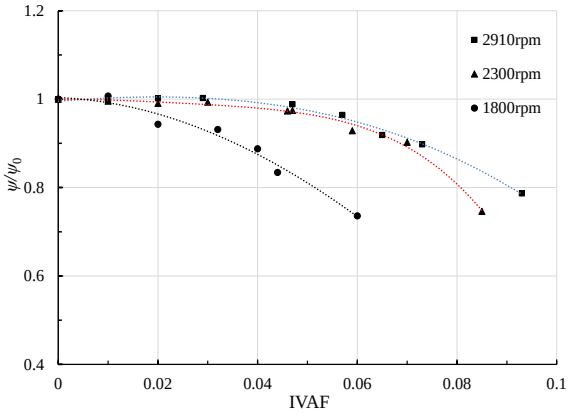

(b) Flow coefficient φ=0.058

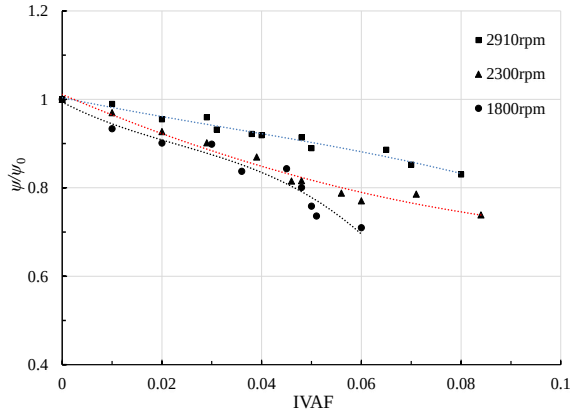

(c) Flow coefficient φ=0.040

Figure 7 Pump performance degradation ratios.

Below φ = 0.04, the ratio ψ/ψ_0 sharply decreases (more than 50%). This value of φ= 0.04 also corresponds roughly to a limiting value for which the theoretical head curve does not any more follow the theoretical straight line corresponding to the hypothesis of no inlet swirl. This sharp head drop, which is observed for low flow rate and high void fraction, is probably related to inlet swirl effects, combined with local reverse flows inside the impeller close to the inlet shroud area as already detected by Schäfer et al. (2015) in an another pump geometry.

Numerical results

Pump performance comparison between the simulation and experiment

Comparisons between simulation and experiment when pump works at pure water condition are shown in Figure 8. For the CFD results, the delivery head was obtained from one averaged revolution of the unsteady calculation. Based on most conditions, the numerical head well agree with the corresponding experimental results. The agreement at the part-load operating points were better than that at the design and over-load operating points, which may be due to the neglected roughness. All of above means that the calculated domain, meshes, boundary condition and numerical turbulence models is suitable for the research.

Performance curves of numerical simulation and experiment with different AVF is shown in Figure 9. Numerical results show that the calculation is quite sensitive to initial bubble diameter value for small flow rates. Numerical results are quite comparable up IAVF= 7% for the adapted bubble diameter.

From experimental investigation, it seems that pump performance is less sensitive to inlet bubble diameter values than numerical results. This result also needs more investigation in order to explain it. The simulation results are believable if choose the right initial bubble diameter.

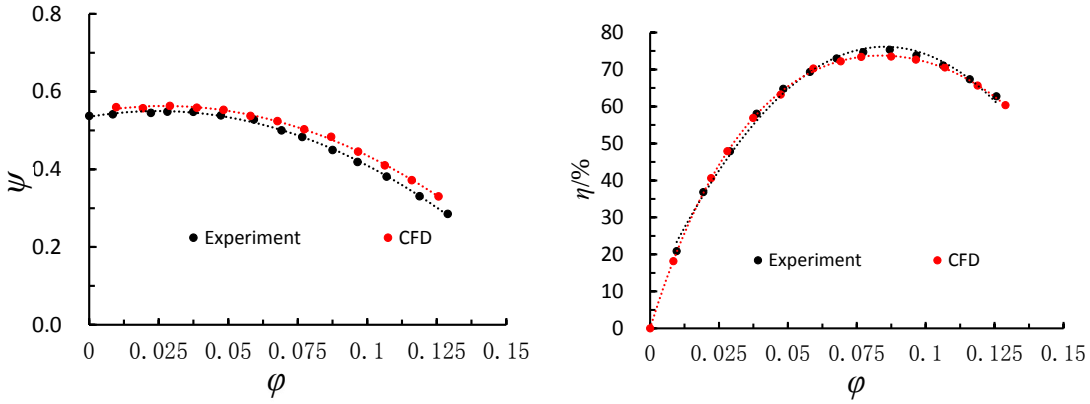

(a) Head (b) Efficiency

Figure 8. Performance curves of numerical simulation and experiment with IAVF=0.

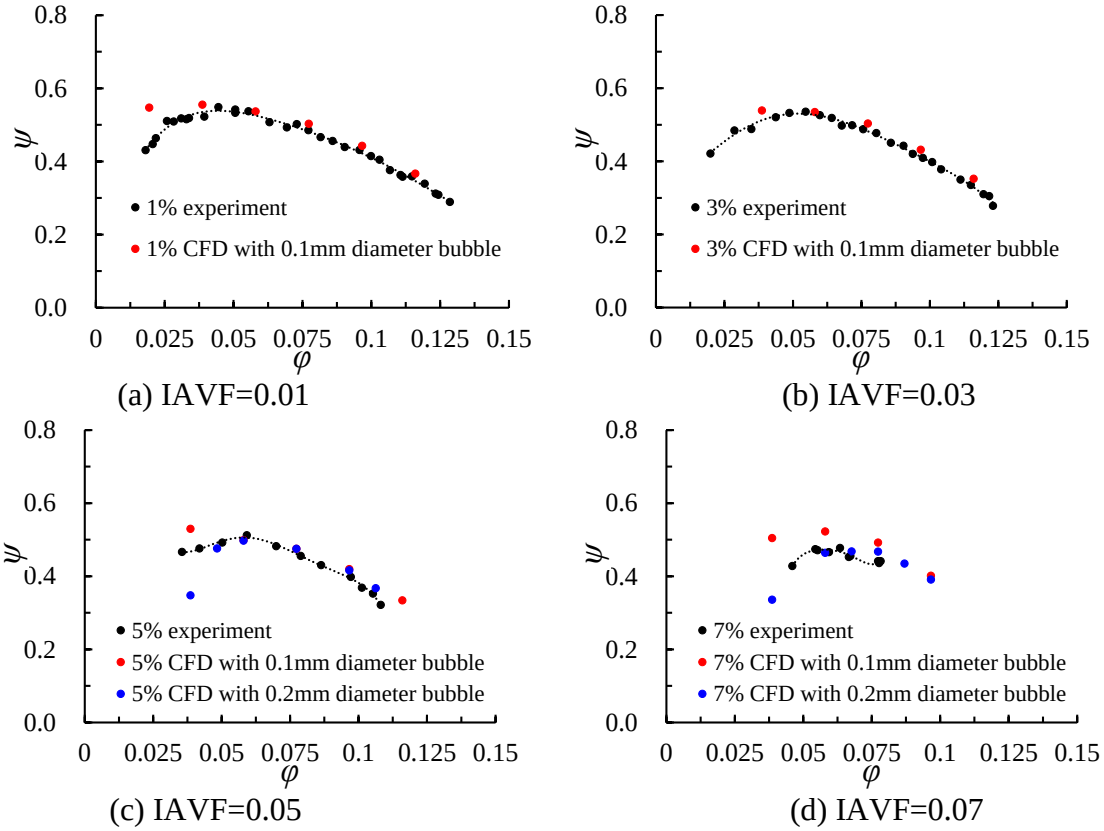

(a) IAVF=0.01 (b) IAVF=0.03

(c) IAVF=0.05 (d) IAVF=0.07

Figure 9. Pump performance for different IAVF values.

CFD results: Flow inside the impeller.

The transport gas-liquid ability of the pump mainly depends on air and water distributions inside the impeller. Table 2 and Table 3 show α distribution on the blade surface and inside the impeller channel for three different flow rates (two below design condition and one at design condition) with three different IAVF values. It can be seen that more air resides on the inlet leading edge near hub and outlet trailing edge near shroud when IAVF is small. Air bubbles distribute on pressure side of the blade and are detained more and more inside the impeller channel near "wake" area when IAVF increase. Air void fraction is bigger on pressure side than suction side in all three flowrates. Bubbles take over 60% part of the channel when IAVF increase to 7% in all three

flowrates, which is probably the reason why pump performance breaks down. Air bubbles are also detected on blade pressure side from leading edge to the middle channel parts. Close to the shroud part of the impeller and near the trailing edge, the biggest α values can be detected. Part of such kind of results has also been shown in Müller's work (2005). Further investigations from numerical results are needed in order to evaluate high loss locations due two phase conditions and on impeller blade static pressure distribution as pointed out in the conclusions of Müller's paper (2005).

Table 2 Air distribution on blade under different IAVF

Flow rate	Scale	IAVF=1%	IAVF=5%	IAVF=7%
$0.6Q_d$	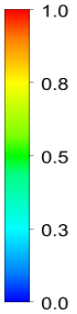	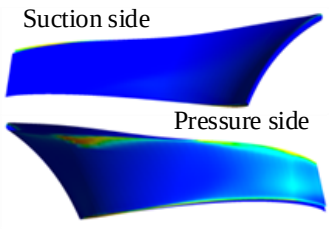	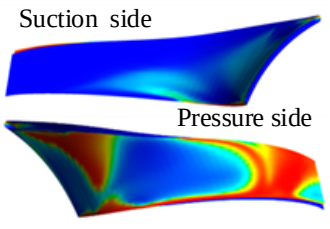	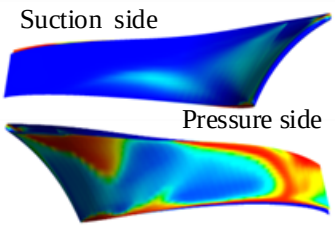
$0.8Q_d$		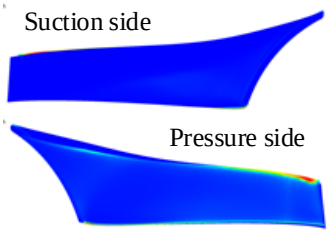	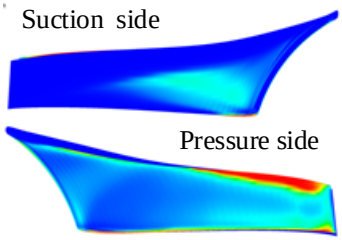	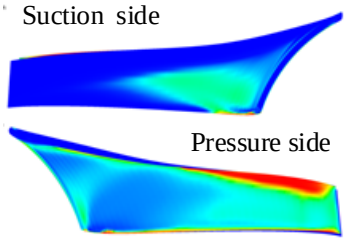
Q_d		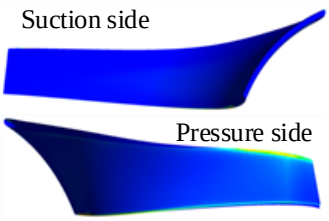	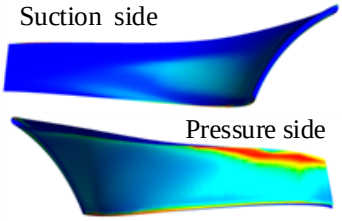	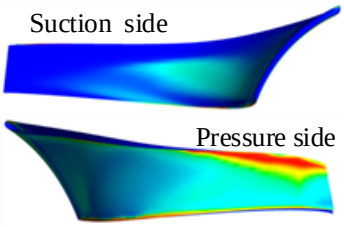

CONCLUSIONS

Experimental overall pump performances have been performed under air water two phase conditions for a low specific centrifugal geometry, for a wide range of rotational speeds. Local flow pattern have been also obtained using CFD results in order to explain the head degradation level when IAVF was increased. The main results are the following:

1. The similarity laws are valid for a range of rotational speed which is compatible with usual pump Reynolds number value above the critical one. The similarity laws can also be applied for air-water two phase flow conditions corresponding to the bubbly flow regime, when IVAF is small. For this flow regime, the theoretical head coefficient versus flow coefficient exhibits a single curve for all rotational speeds and IAVF values up to 7%.
2. Pump performance degradation is more pronounced for low flow rates compared to high flow rates. The starting point of severe pump degradation rate is related a specific flow coefficient, which value corresponds to the change of the slope of the theoretical head curve.
3. Compared with existing experimental results for 2D impeller shapes, the present 3D impeller pump geometry head degradation is quite small (less than 1%) within IAVF values below 5% between $0.7Q_d$ and Q_d.
4. Local numerical results inside the impeller blade passages give some explanation about this last point and describe the air-water flow pattern change just before the experimental pump

breakdown. Particle fluid model with interface transfer terms looks quite suitable to evaluate pump performance degradation up to IAVF values of 7%.

5. Maximum experimental IAVF of 10% can be reached before pump breakdown only for initial inlet flow conditions higher that best efficiency ones. Numerical approach always fails using high IAVF inlet conditions.
6. More analysis on loss increase and static pressure on blade surface are still under investigations in order to determine the critical parts on the pump with regards on its two-phase flow capability.

Table 3 Contour planes when α is above 20% for different IAVF values

Flow rate	Scale	IAVF=1%	IAVF=5%	IAVF=7%
$0.6Q_d$	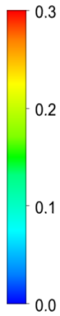	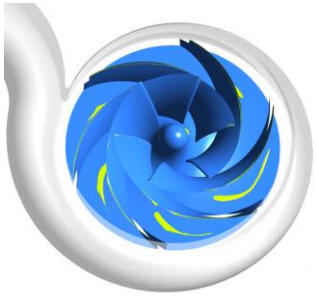	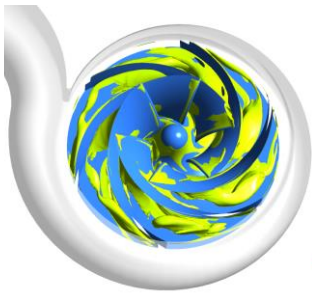	
$0.8Q_d$		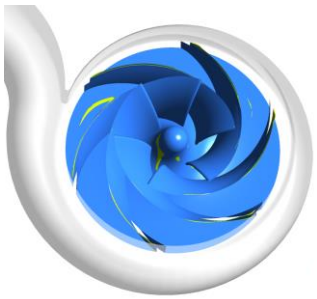	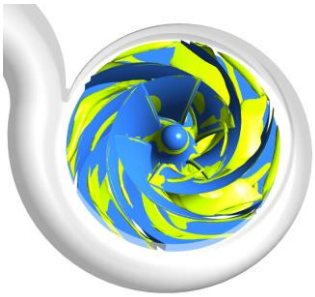	
Q_d		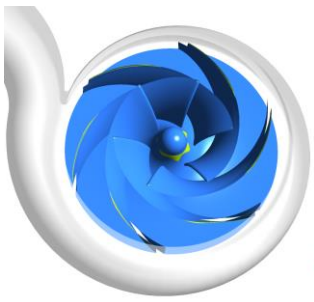	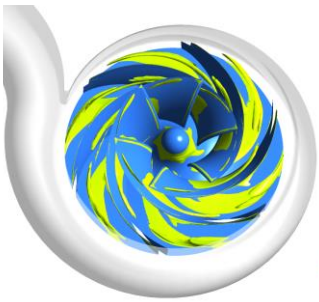	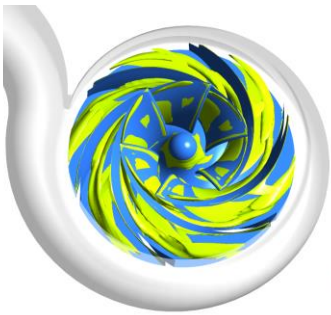

ACKNOWLEDGEMENTS

The authors gratefully acknowledge the financial support by National Natural Science Foundation of China (51509108), Natural Science Foundation of Jiangsu Province (BK20150516), China Postdoctoral Science Foundation Funded Project (2015M581735, 2016T90422) and Senior Talent Foundation of Jiangsu University (15JDG048). The authors also acknowledge ATTAG-Association Technique des Turbines àGaz- for it financial support for the presentation of this paper.

REFERENCES

Barrios, L., M. G. Prado, (2009). "Modeling two phase flow inside an electrical submersible pump stage". ASME 2009 28th International Conference on Ocean, Offshore and Arctic Engineering. Honolulu, Hawaii, USA: ASME, 469-484.

Clarke, A.P., ISSA, R. I., (1995)." Numerical prediction of bubble flow in a centrifugal pump". Multiphase Flow, 1995:175-181.

Caridad, J., Kenyery, F., (2004). "CFD Analysis of electric submersible pumps (ESP) handling two-phase mixtures". Journal of Energy Resources Technology (ASME), 126.2, 99-104.

Furuya, O., (1985)." An analytical model for prediction of two-phase (non condensable) flow pump performance". ASME Journal of Fluid Engineering, 107(1): 139-147.

Kim, J.H., Duffey, R.B., Belloni, P., (1985). "On centrifugal pump head degradation in two-phase flow. Design method for two-phase flow in turbomachinery". ASME Mechanics Conference, 26 Albuquerque, NM.

Mikielewicz. J., Wilson. D.G., Chan. T.C., Goldfinch. A.L.,(1978)."A method for correlating the characteristics of centrifugal pumps in two-phase flow". ASME Journal of fluids Engineering, 100, December 1978.

Minemura, K., Murakami,M., Katagiri,H., (1985). "Characteristics of Centrifugal Pumps Handling Air-Water Mixtures and Size of Air Bubbles in Pump Impellers". Bulletin of JSME, 28(244): 2310-2318.

Minemura,K., Kinoshita,K., Ihara,M., Furukawa,H., Egashira,K., (1995). "Effects of outlet blade angle of centrifugal pump on the pump performance under air-water two-phase flow conditions". ASME energy sources technology conference and exhibition, Houston, TX, Pipeline Engineering, PD-Volume 69: 113-117.

Müller. T., (2015). "Numerical 3D RANS Simulation of Gas-Liquid Flow in a Centrifugal Pump with an Euler-Euler Two-Phase Model and a Dispersed Phase Distribution", 11thEuropean Conference on Turbomachinery Fluid dynamics & Thermodynamics,ETC11, March 23-27, ETC2015-076, Madrid, Spain.

Murakami, M., Minemura, K., (1974a). "Effects of entrained air on the performance of a cent rifugal pump (First report, performance and flow conditions)". Bulletin of the ASME, 1047-1055.

Murakami, M., Minemura, K., (1974b). "Effects of entrained air on the performance of a centrifugal pump (Second report, effects of number of blades)". Bulletin of the ASME, 1286-1295.

Sato, S., Furukawa, A., Takamatsu, Y., (1996). "Air-Water Two-Phase Flow Performance of Centrifugal Pump Impellers with Various Blade Angles".
ASME International Journal, 39.2, 223-229.

Schäfer, T., Bieberle, A., Neumann, M., Hampel, U., (2015). "Application of gamma-ray computed tomography for the analysis of gas holdup distributions in centrifugal pumps". Flow Measurement and Instrumentation, 46, 262–267.

Suryawijaya, P., Kosyna, G., (2001). "Unsteady Measurement of Static Pressure On the Impeller Blade Surfaces and Optical Observation on Centrifugal Pumps Under Varying Liquid/Gas Two-Phase Flow Condition". Journal of Computational and Applied Mechanics, 2.1, D9-D18.

Thum, D., Hellmann, H., Sauer, M., (2006). "Influence of the Patterns of Liquid-Gas Flows on Multiphase-Pumping of Radial Centrifugal Pumps". 5th North American Conference on Multiphase Technology. 79-90.

Thomas, S., André, B., Martin, N., Uwe, H.,(2015). "Application of gamma-ray computed tomography for the analysis of gas holdup distributions in centrifugal pumps". Flow Measurement and Instrumentation, 46, 262-267.